DR SHUANGHE CAO (Orcid ID : 0000-0002-2905-0728)

PROFESSOR CHENGCAI CHU (Orcid ID : 0000-0001-8097-6115)

Article type : Original Article

The florigen interactor BdES43 represses flowering in the model temperate grass *Brachypodium distachyon*

Shuanghe Cao[1#*], Xumei Luo[1#], Li Xie[1#], Caixia Gao[2], Daowen Wang[2], Ben F. Holt III[3], Hao Lin[4], Chengcai Chu[2], Xianchun Xia[1]

[1]Institute of Crop Sciences, National Wheat Improvement Center, Chinese Academy of Agricultural Sciences (CAAS), 12 Zhongguancun South Street, Beijing 100081, China

[2]Institute of Genetics and Developmental Biology, Chinese Academy of Sciences (CAS), No. 1 West Beichen Road, Chaoyang District, Beijing 100101, China

[3]Department of Microbiology and Plant Biology, University of Oklahoma, 770 Van Vleet Oval, Norman, OK 73019, USA

[4]Biotechnology Research Institute, Chinese Academy of Agricultural Sciences (CAAS), 12 Zhongguancun South Street, Haidian District, Beijing 100081, China

[#]Equal contributions

[*]Correspondence should be addressed to S.C. (email: caoshuanghe@caas.cn)

Running title: Florigen may participate in chromatin remodeling

Key words: *Brachypodium*, *BdES43*, H3K4me3, florigen, flowering time, gene editing

Summary

FLOWERING LOCUS T (FT) protein, physiologically florigen, has been identified as a system integrator of numerous flowering time pathways in many studies and its homologs are found throughout the plant lineage. It is important to uncover how precisely florigenic homologs contribute to flowering initiation and how these factors interact genetically. Here we dissected the function of *Brachypodium FT* orthologs *BdFTL1* and *BdFTL2* using overexpression and gene-editing experiments. Transgenic assays showed that both *BdFTL1* and *BdFTL2* could promote flowering, whereas *BdFTL2* was essential for flowering initiation. Notably, *BdFTL1* is subject to alternative splicing (AS) and its transcriptional level and AS are significantly affected by *BdFTL2*. Additionally, BdFTL2 could bind with the PHD-containing protein BdES43, an H3K4me3 reader. Furthermore, *BdES43* was antagonistic to *BdFTL2* in flowering initiation in a transcription-dependent manner and significantly affected *BdFTL1* expression. BdFTL2, BdES43 and H3K4me3 also had highly similar distribution patterns within the *BdFTL1* locus, indicating their interplay in regulating target genes. Taken together, florigen BdFTL2 functions as a potential epigenetic effector of *BdFTL1* by interacting with a BdES43-H3K4me3 complex. This finding provides an additional insight for the regulatory mechanism underlying the multifaceted roles of florigen.

Introduction

Flowering is crucial for the reproductive success of plants, and the proper timing of flowering determines environmental adaptation and agronomic productivity in crop plants. Genetic regulation of flowering mainly includes five pathways: photoperiod, vernalization, gibberellin, autonomy and age (Fornara *et al.* 2010; Pin and Nilsson, 2012). FT protein, physiologically florigen, functions as a hub to determine flowering initiation in all plants where flowering-time genes have been investigated (Fornara *et al.* 2010; Srikanth and Schmid 2011; Wigge 2011; Andres and Coupland 2012; Pin and Nilsson 2012; Song *et al*. 2015).

Brachypodium distachyon (hereafter *Brachypodium*) is a wild grass species and a model of temperate crops, such as wheat and barley (IBI 2010; Brkljacic *et al*. 2011; IWGSC 2014). Comparative genomic analyses identified 18 *FT* homologs in the *Brachypodium* accession Bd21, and *BdFTL1* (Bradi2g07070) and *BdFTL2* (Bradi1g48830) had the highest similarity with previously reported flower-promoting *FT* genes (Higgins *et al*. 2010). Transcriptional analyses showed a high association of *BdFTL2* with the flowering time of distinct accessions from different areas (Schwartz *et al*. 2010). Recently, *BdFTL2* was identified as a candidate gene underlying a major QTL for flowering time (Bettgenhaeuser *et al*. 2017). Additionally, overexpression of *BdFTL2* promoted flowering (Ream *et al*. 2014) and RNAi experiments confirmed that *BdFTL2* was critical in controlling flowering time (Lv *et al*. 2014). Furthermore, both *BdFTL1* and *BdFTL2* were targeted by miR5200 and could promote flowering, indicating redundant function of the two *FT*-like genes in flowering (Wu *et al*. 2013). Overexpression of *BdFTL2* could also rescue the non-flowering *phyC* mutant phenotype, consistent with it being an important downstream photoperiod integrator (Woods *et al*. 2014). Further, *BdFTL1* was undetectable in the *phyC* background; thus, loss of *BdFTL1* expression might also contribute to the delayed flowering phenotype of the *phyC* mutant (Woods *et al*. 2014). However, it is still unclear how precisely florigenic homologs contribute to flowering initiation and how these factors interact genetically. Here our objective was to better understand the individual effects of *BdFTL1* and *BdFTL2* on flowering, their genetic relationship and regulatory machinery.

Results

BdFTL1 and BdFTL2 have the highest homology with known florigens

To examine the homologs of *FT* genes in *Brachypodium*, we performed a phylogenetic analysis across major crops in the temperate grass family as well as the model plants *Arabidopsis* and rice. In the phylogenetic tree, most function-validated FT homologs are grouped in the same monophyletic clade and there are two members for each species, except that rice possessed three due to a tandem duplication event **(Figure 1A; Dataset S1)**. Among them, BdFTL1 and BdFTL2 are the two FT homologs with the highest similarity to known florigens, such as AtFT and Hd3a (Corbesier *et al*. 2007; Tamaki *et al*. 2007). Genomic synteny analyses also validated that *BdFTL1* and *BdFTL2* were orthologous with rice florigen genes **(Figures 1B and 1C; Dataset S2)**.

Both *BdFTL1* and *BdFTL2* enable flowering initiation

In previous studies, overexpression (OE) experiments demonstrated that both *BdFTL1* (Wu *et al*. 2013) and *BdFTL2* (Wu *et al*. 2013; Lv *et al*. 2014; Ream *et al*. 2014) sufficed to promote flowering. We observed the same result in initial experiments using the ZmUbi promoter **(Figure 2A)**, however, as previously reported, no seeds were obtained because the T_0 lines flowered too early to presumably generate the biomass needed for seed production (Wu *et al*. 2013; Lv *et al*. 2014). Because the 35S promoter drives considerably lower expression than ZmUbi in grasses (Christensen *et al*. 1992; Alves *et al*. 2009), we developed 35S promoter-driven *BdFTL1* and *BdFTL2* constructs. Ten OE lines each for *BdFTL1* and *BdFTL2* were used to investigate phenotypic data. As with the ZmUbi-driven constructs, both *p35S:BdFTL1* and *p35S:BdFTL2* significantly promoted early flowering **(Figures 2B and 2C; Dataset S3)**. Additionally, we successfully obtained transgenic seeds, facilitating the following investigations.

BdFTL2 plays a pivotal role in flowering initiation

To further reveal the respective effects of *BdFTL1* and *BdFTL2* on flowering, we created gene-specific knockout (KO) lines using TALEN technology **(Figure S1).** Ten KO (truncation and/or frameshifts) homozygous lines each for *BdFTL1* and *BdFTL2* were used to investigate flowering time. Strikingly, *BdFTL2*-KO lines did not flower for approximately three months under

inductive long day (LD) conditions, whereas *BdFTL1*-KO lines had comparable flowering times to the wild type (WT) **(*P* = 0.0540 in Dataset S3; Figures 2D and 2E)** although *BdFTL1* KO delayed flowering by more than 5 days compared with WT **(Dataset S3)**. We additionally examined the flowering time phenotypes of eight *BdFTL1* and *BdFTL2* double mutants. The flowering times of the double mutant lines were similar to that of *BdFTL2*-KO lines **(*P* = 0.0540 in Dataset S3; Figures 2D and 2E)**. Moreover, we compared the flowering time of *BdFTL1*-KO, *BdFTL2*-KO and WT lines under short day conditions and observed that *BdFTL2*-KO lines also flower later than WT lines, while *BdFTL1*-KO lines has similar flowering time to WT lines (**Figure S2**). Thus, *BdFTL1* appears to be dispensable for flowering, but *BdFTL2* is critical to initiate flowering.

BdFTL1 and *BdFTL2* display similar transcriptional patterns

To explore the underlying reason for the differences between *BdFTL1* and *BdFTL2* in flowering initiation, we investigated their transcription patterns under inductive LD conditions. From previous research, we expected florigenic *FT* expression in leaves, with a significant daily response to photoperiod and a gradual increase prior to flowering (Corbesier *et al*. 2007; Tamaki *et al*. 2007). Initially we tested the transcriptional activities of *BdFTL1* and *BdFTL2* in different tissues and observed similar tissue-specific expression profiles: mainly expressing in leaves, relatively low transcriptional activity in stems, and rarely expressing in roots **(Figure 3A; Paired t-test *P* = 0.0578 in Table S1)**. We further investigated the time-course transcriptional variation of *BdFTL1* and *BdFTL2* over a full day under LD conditions. Both genes had significant responses to the light/dark shift with similar transcriptional patterns, including an incremental increase in mRNA accumulation, peaking at end of day, and then a gradual decline in the dark **(Figure 3B; Paired t-test *P* = 0.1489 in Table S1)**. The transcriptional levels of *BdFTL1* and *BdFTL2* in different developmental phases were also measured. qPCR indicated that *BdFTL2* transcription activity was comparatively stronger than *BdFTL1* in the corresponding period; however, their transcription activities in different developmental phases were similar - i.e., increasing over developmental time before flowering **(Figure 3C; Paired t-test *P* = 0.7186 in Table S1)**. Overall,

BdFTL1 and *BdFTL2* had similar transcription patterns in different tissues, developmental phases, and during responses to the light/dark shift, indicating that transcriptional regulation was not likely to be the key element causing large functional differences in flowering.

BdFTL1 is subject to mRNA alternative splicing

Since transcriptional regulation was not the obvious determinant for the functional discrepancy between *BdFTL1* and *BdFTL2*, we compared their post-transcriptional activities. Deep sequencing showed that approximately 42-48% of genes underwent alternative splicing (AS) of mRNA in *Arabidopsis* and rice (Filichkin *et al*. 2010; Lu *et al*. 2010b). In addition, Qin et al (2017) identified an AS event in *BdFTL1* locus. As such, we explored AS events in the *BdFTL1* and *BdFTL2* loci. Coding DNA sequence (CDS) identification showed that *BdFTL1* was subject to AS under LD conditions **(Figure 3D)**, whereas no AS was observed at the *BdFTL2* locus **(Figure 3E)**. The AS event at *BdFTL1* generated a transcript isoform with a premature stop codon that was predominant for three weeks after germination **(Figures 3D and S3)**. This suggested that AS of *BdFTL1* might impair its function in flowering during these early developmental stages.

BdFTL2 influences both transcription and alternative splicing of _BdFTL1_

The AS event in *BdFTL1* resulted in the late appearance of the functional transcript, which in WT lines gradually increased to high levels and became predominant five weeks after germination **(Figure 3D)**. Therefore, five-week old seedlings should possess flowering competency even in a *BdFTL2* loss of function mutant. However, *BdFTL2*-KO lines with a native *BdFTL1* did not flower for ~3 months under inductive LD conditions **(Figures 2D and 2E)**. We speculated that the functional transcript of *BdFTL1* in *BdFTL2*-KO lines was expressed at lower levels than in WT lines. To test this hypothesis, we firstly compared *BdFTL1* transcriptional levels between *BdFTL2* knockout and WT lines. qPCR indicated that *BdFTL1* in *BdFTL2*-KO lines had much lower transcriptional levels than that in WT lines, consistent with the previously published data from the analysis of *BdFTL2* RNAi lines **(Figure 3F)** (Lv *et al*. 2014). Moreover, due to AS, the *BdFTL1* functional transcript was almost undetectable in *BdFTL2*-KO lines up to 10 weeks after germination **(Figure 3G)**. *BdFTL2* overexpression could also promote the expression of *BdFTL1*

(**Figure S4**). Thus, *BdFTL2* directly or indirectly regulates the transcriptional activity and AS of *BdFTL1*.

BdFTL2 interacts with BdES43, an H3K4me3 reader

Since *BdFTL2* greatly affects *BdFTL1* transcriptional activity and AS, we further investigated the potential role of *BdFTL2* in regulating *BdFTL1*. Previous research showed that FT usually regulates downstream targets by binding other proteins such as FD-like and 14-3-3-like proteins (Taoka *et al*. 2013). To identify proteins interacting with BdFTL2, we performed yeast two-hybrid (Y2H) screens using a previously constructed *Brachypodium* Y2H library (Cao *et al*. 2011b). Six representative partners of BdFTL2 were identified, including a previously identified mtN19 homolog (Adrian 2009), and new partners BdES43, Bd2OG, BdSTN7, BdB2 and BdDUF886 **(Figure 4A; Table S2)**. However, we did not isolate the expected FD-like and 14-3-3-like proteins as partners of BdFTL2 in this library screen. The Y2H library used in this study was constructed from two-week old seedlings (Cao *et al*. 2011b) and transcriptional analyses showed that *BdFDL2* and *Bd14-3-3B* had very low transcriptional levels in two-week-old shoot tissues **(Figure S5A)**, which might account for why they were not identified as interactors in the screen. Therefore we additionally isolated the four *14-3-3* and two *FD* homologs in *Brachypodium* based on previous reports in wheat (Li and Dubcovsky 2008; Li *et al*. 2015) and directly tested their potential interactions with BdFTL2 by Y2H; only BdFDL2 and Bd14-3-3B were observed to bind with BdFTL2 **(Figure S5B)**.

Interestingly, among the newly isolated partners of BdFTL2, BdES43 contains bromo-adjacent homology (BAH) and plant homeodomain Zn finger (PHD) domains **(Figure S6A)**. The PHD domain is thought to mediate protein-protein interactions and usually appears in transcriptional regulators involved in chromatin remodeling (Wysocka *et al*. 2006; de la Paz Sanchez and Gutierrez 2009; López-González *et al*. 2014, Qian *et al.* 2018). Alignment and homology analyses showed that BdES43 was highly similar to AtEBS and AtSHL, especially in functionally important amino acid residues of the BAH and PHD domains, recognizing H3K27me3 and H3K4me3, respectively **(Figures S6A, S6B, and S6C)** (Qian *et al*, 2018). Bimolecular

fluorescence complementation (BiFC), pull-down and luciferase complementation (LUC) experiments all confirmed interactions between BdFTL2 and BdES43 **(Figures 4B, 4C and 4D)**. Pull-down assays validated that BdES43 could bind with native H3K4me3 extracted from *Brachypodium* seedlings, but hardly interacted with H3K27me3 **(Figures 4E and S7),** which is consistent with the previously reported result in López-González *et al*. (2014). Moreover, *BdES43* overexpression (*BdES43*-OE) resulted in late flowering and a dwarf stature under inductive LD conditions **(Figure 4F)**. H3K4me3 is also known to be associated with transcriptional regulation and AS (Spies *et al*. 2009; Tian *et al*. 2011; Ding *et al*. 2012; Huang *et al*. 2012; Davie *et al*. 2016). Thus, this data suggests that the *BdFTL2* regulation of *BdFTL1* may be mediated by interactions with the BdES43-H3K4me3 complex.

***BdES43* and *BdFTL2* have opposite transcription patterns in flower initiation**

BdFTL2-OE greatly promoted flowering, whereas *BdES43*-OE caused extremely late flowering **(Figure 4F)**. Additionally, BdFTL2 could physically bind with BdES43 **(Figures 4B, 4C and 4D)**, suggesting their respective functions in flowering are coupled through their physical interaction. To probe the genetic relationship of *BdFTL2* and *BdES43* in flowering, their expression patterns in different background lines were additionally investigated and compared. We observed that *BdFTL2* transcription in WT lines increased with developmental progress, as in the experiments above **(Figure 3C)**, whereas *BdES43* expression was constitutively highly expressed in leaves throughout development **(Figure S6E)**. Accordingly, the WT line gradually gained flowering capacity with developmental progress and flowered at the expected phase. In the *BdFTL2*-OE lines, plants flowered early while *BdES43* retained its normal constitutive expression **(Figures 2A and S6F)**. In the converse experiment, *BdES43*-OE plants flowered extremely late and have significantly reduced *BdFTL2* expression compared to the WT line **(Figures 4F, 4G and S6G)**. Thus, the delayed flowering of *BdES43*-OE is likely resulted from the reduced levels of *BdFTL2* transcription during the first 8-9 weeks post seed germination. These findings verified that *BdFTL2* and *BdES43* have antagonistic effects on flowering initiation and determine flowering in a transcription-dependent manner.

BdES43 affects *BdFTL1* expression

Since *BdFTL2* can alter *BdFTL1* expression, likely through its interaction with *BdES43*, it is necessary to investigate the *BdFTL1* expression pattern in *BdES43*-OE lines. Transcriptional pattern assays in *BdES43*-OE lines showed that *BdFTL1* transcripts were barely detectable for 7 weeks post germination and its AS-derived transcripts were predominant up to 9 weeks after germination **(Figures 4G and Figure S6D)**. Thus, *BdES43* alterations had an obvious effect on transcription and AS of *BdFTL1*. ChIP-qPCR assays also showed BdES43 and H3K4me3 had similar distribution patterns at the *BdFTL1* locus: higher affinity with the promoter and AS region than with the more downstream regions of the *BdFTL1* locus **(Figures 5A and 5B; Table S3)**. Our data collectively suggested that *BdES43* might regulate the transcription and AS of *BdFTL1* by interacting with H3K4me3.

BdFTL2, BdES43 and H3K4me3 have similar enrichment patterns in the *BdFTL1* locus

To further investigate whether BdFTL2 can bind the *BdFTL1* locus, ChIP experiments were performed using *BdFTL2*-OE lines. ChIP-qPCR assays showed that BdFTL2 and H3K4me3 physically bind to similar regions of the *BdFTL1* locus, consistent with that of BdES43 **(Figures 5A, 5B and 5C; Table S3)**. We also detected the presence of H3K4me3 at the *BdFTL1* locus in the WT lines during different developmental stages. The distributional enrichment of H3K4me3 was higher in the promoter and AS regions than in more distal positions of *BdFTL1* and exhibited roughly parallel changes at each site during development **(Figure 5D)**. Therefore, co-localization of BdFTL2, BdES43, and H3K4me3 in the promoter and AS region of *BdFTL1*, as well as their genetic and physical interactions described above, strongly suggests they synergistically regulate the transcription and AS of *BdFTL1*. Considering that H3K27me3 is also known to be involved in alternative splicing and transcription (Luco *et al*. 2010; Mercer *et al*. 2013), we also investigated H3K27me3 distribution within *BdFTL1* locus and found that its enrichment in the promoter and around alternative splicing site is not significantly higher than that in more distal positions of *BdFTL1* **(Figures 5B, 5C and 5E)**. Moreover, we compared the distribution of BdES43, H3K27me3 and H3K4me3 within *BdFTL2* locus using the two-week-old leaves of BdES43-OE

lines **(Figure S8)**. ChIP-qPCR showed that H3K27me3 enrichment in the promoter of *BdFTL2* was significantly higher than other distal regions, whereas H3K4me3 and BdES43 were not. Thus, H3K27me3 may have effect on the expression of *BdFTL2*, while H3K4me3 and *BdES43* probably are irrelevant with *BdFTL2*.

Discussion

In the present study, we achieved the functional dissection of *Brachypodium FT* homologs *BdFTL1* and *BdFTL2* by transgenic assays. Although there is no statistically significant difference in flowering time between *BdFTL1* KO and WT lines, *BdFTL1* KO delayed flowering for more than 5 days compared to WT **(Dataset S3).** Additionally, *BdFTL1* overexpression can greatly accelerate flowering just as *BdFTL2*. Furthermore, *BdFTL1* is subject to AS in WT lines, probably accounting for the comparable flowering time between its KO and WT lines. Collectively, *BdFTL1* is a promoter of flowering just as *BdFTL2* and its function in accelerating flowering may be impaired by the AS event. We found that *BdFTL2* has a significant effect on AS and transcription activity of *BdFTL1* through transgenic KO and OE experiments **(Figure 3G)**. Most importantly, we uncovered that BdFTL2 can bind to BdES43, and BdES43 can also interact with H3K4me3. *BdFTL2* and *BdES43* have opposite effects on the transcriptional initiation of *BdFTL1* and flowering. Additionally, BdFTL2, BdES43 and H3K4me3 successively interact and have similar distribution patterns at the *BdFTL1* locus: higher enrichment in the promoter and AS regions than in more distal positions **(Figures 5A, 5B, 5C and 5D)**. Thus, it is of biological significance to reveal regulatory mechanism underlying *BdFTL1* for the flowering control in *Brachypodium*.

Evidence for coupling between transcriptional and splicing machinery is rapidly accumulating, especially for genes with long introns which may severely reduce the transcription elongation rate and increase AS efficiency (Bell *et al*. 1998; Hatton *et al*. 1998; Burnette *et al*. 2005; Fox-Walsh *et al*. 2005; Graveley 2005; Kim *et al*. 2006; Mcguire 2008; Roy *et al*. 2008; Kandul and Noor 2009; Pandya-Jones and Black 2009; Spies *et al*. 2009; Shukla and Oberdoerffer 2012). Most published splicing events of constitutive exons also are co-transcriptional in a general 5′ to 3′ order

- i.e., the closer the splicing site is to the 5′ terminal region of a gene, the higher the possibility that AS couples with the transcription process (Pandya-Jones and Black 2009). The target AS site of *BdFTL1* lies in the first exon, followed by a long downstream intron **(Figure S3)**. We thus speculate that the AS of *BdFTL1* is co-transcriptional. Considerable evidence has revealed that transcription elongation rates are tightly related to chromatin structure and directly involved in the AS events in co-transcriptional splicing processes (Shukla and Oberdoerffer 2012; Braunschweig *et al*. 2013; Kornblihtt *et al*. 2013; Bentley 2014). Moreover, it is well known that H3K4 methylation exerts a significant influence on gene transcription and AS (Burnette *et al*. 2005; Spies *et al*. 2009; Tian *et al*. 2011; Ding *et al*. 2012; Huang *et al*. 2012; Ong-Abdullah *et al*. 2015; Davie *et al*. 2016). Here we present a model for *BdFTL2* regulation of *BdFTL1* based on our experimental evidence and above reasoning **(Figure 6A)**. According to our model, a BdES43 complex binds with H3K4me3 in the early plant developmental phases to repress transcription initiation and elongation rates at the *BdFTL1* locus by chromatin remodeling. The elongation rate is so slow that long dwell times for coupling transcription and splicing in the target splicing site promotes the occurrence of AS of *BdFTL1*. Consequently, the transcriptional efficiency of *BdFTL1* is low and AS occurs frequently in the early growth stages. As development proceeds, *BdFTL2* expression increases and influences the function of the BdES43 complex through their interaction. As a result, the interaction triggers the derepression of *BdFTL1* transcription and a concomitant reduction in AS.

In this study, the interaction between BdFTL2 and BdES43 plays the central role in tracking how *BdFTL2* regulates *BdFTL1*. It has been proposed in the model above that BdFTL2 modulates the structure of the BdES43 complex and alters its function. Conversely, BdES43 should also affect the function of BdFTL2 concurrently. We achieved *BdFTL2*-OE in the *BdFTL1*-KO background (*BdFTL2*-OE/*BdFTL1*-KO) through hybridization of *BdFTL2*-OE and *BdFTL1*-KO lines. The *BdFTL2*-OE/*BdFTL1*-KO lines flowered a little later than *BdFTL2*-OE in wild-type lines and much earlier than *BdFTL1*-KO and wild type lines **(Figure S9)**, suggesting that *BdFTL2* partially regulates flowering via *BdFTL1* regulation. Additionally, BdFTL2 might form a flowering-activating complex by interacting with *Brachypodium* 14-3-3 and FD homologs **(Figure**

S5B), indicating that BdFTL2 controls flowering through multiple molecular regulatory pathways. Recently, it was shown that the overexpression of a *BdFTL1* splice transcript repressed flowering by preventing the assembly of a functional flowering-activating complex containing BdFTL1, BdFTL2, 14-3-3 and FD proteins, providing additional cues to their relationships in flowering initiation (Qin *et al*. 2017). It is thus possible that BdES43 sequesters BdFTL2 from the flowering-activating complex to cause late flowering. We speculated that the competitive binding of BdES43 and the homologues of FD or/and 14-3-3 with BdFTL1 may be an important cause of extremely late flowering of *BdES43*-OE lines **(Figure 6B)**. In near future, we will test the hypothesis through protein competitive interaction (e.g. yeast-three -hybrid or pull-down methods) and transgenic assays.

AtEBS and AtSHL, homologs of BdES43, interact genetically with numerous flowering-related epigenetic modifiers, such as HDACs with deacetylase activity, ATX1/ATXR7 with putative Set 1 class H3K4 methylase activity, and EFL6 and HUMONJI4/14(JMJ4/JMJ14) with demethylase activity (Tamada *et al*. 2009; Lu *et al*. 2010a; Yu *et al*. 2011; He 2012; Yang *et al*. 2012; López-González *et al*. 2014). Additionally, there is evidence that AtEBS can bind physically with the HDAC family members, HDA6 and HDA19 (López-González *et al*. 2014). A number of other PHD proteins have also been shown to control gene expression by recognizing H3K4me3 and recruiting epigenetic factors that can activate or repress the transcription of underlying genes (Shi *et al*. 2006; Wysocka *et al*. 2006; de la Sanchez and Gutierrez 2009; He 2012; Rincon-Arano *et al*. 2012; Molitor *et al*. 2014). Therefore, there is every reason to believe that BdFTL2 affects the BdES43 complex by recruiting chromatin-remodeling factors. As such, it is conceivable that BdFTL2-BdES3-H3K4me3 in the nucleosome is not only a structural unit, but also a signaling platform. Further experiments are necessary to address this question.

In addition to flowering, FT has also been identified as a major regulatory factor in a wide range of developmental processes including fruit set, vegetative growth, stomatal control, and tuberization (Pin and Nilsson 2012; Navarro *et al*. 2015). Here we revealed that the FT ortholog BdFTL2 is involved in chromatin remodeling. This finding fits well with the known roles for FT in the

regulation of different developmental processes and supplies an additional entry point to explore the molecular basis of its pleiotropic effects.

Materials and Methods

Plant material, growth conditions and phenotype characterizations

Brachypodium accession Bd21 was supplied kindly by Prof. Ben Holt III in Oklahoma of University, and used as the recipient for overexpression and knockout of target genes. Seeds were imbibed overnight in darkness between wet paper towels at room temperature and then sown in soil. Seedlings were grown in a growth chamber with 16 h of light per day (long day) and light intensity of 150 μE provided by cool-white tubes. The day/night temperature pattern in the growth chamber was 22/18 °C. Flowering time was measured as the number of days from seed germination to heading of the main stem.

Transgenic experiments for overexpression and knockout

Gateway-compatible ZmUbi-driven pGW101-pBI and CaMV35S-driven pEarleyGate101 vectors were used to overexpress genes of interest. The coding sequences of *BdFTL1* and *BdFTL2* for overexpression experiments are the same as the annotation of Bradi2g07070 and Bradi1g48830, respectively, in BdGDB (http://plantgdb.org/BdGDB/). TALEN vector construction and activity assays in protoplasts were performed as previously described (Shan *et al*. 2013). To construct the TALEN vector, candidate sites were used as queries to perform BLAST against *Brachypodium* genome and were also identified by the TAL Effector-Nucleotide Targeter 2.0 program (https://tale-nt.cac.cornell.edu/), which will guarantee that the target sites is unique and is of low-identity with other regions (Doyle *et al*. 2012). TALEN repeat arrays were listed in **Dataset S4** and were constructed using the Golden Gate method (Zhang *et al*., 2012). Each TALEN recognition sequence contained a restriction enzyme site within the spacer region in favor of identification for applicable constructs and positive lines (**Dataset S4**). TALEN repeat arrays were cloned into expression vector pZHY051 and then transfer into protoplasts using polyethylene glycol (PEG) (Zhang *et al*., 2012). The nuclease activity directed by the resulting constructs was

assessed through PCR/RE assays as described in Shan *et al*. (2013). The transformed protoplasts were incubated for 48 hours and were used to extract genomic DNA. The PCR products encompassing each target site were digested by restriction enzymes and visualized in agarose gel. The PCR amplicons were then cloned and sequenced to confirm the mutations. *Agrobacterium*-mediated transformation was carried out following a previously described procedure with slight modifications i.e. longer (15 min) desiccation treatment after inoculation of callus with *Agrobacterium* and coculturing callus with *Agrobacterium* at lower temperature (21 °C) to reduce excessive proliferation of *Agrobacterium* (Alves *et al.* 2009). The target plants were identified by PCR/RE assays just as described above. The mutant lines were identified with agarose gel electrophoresis and sequencing **(Figure S1)**. To determine whether there are off-target events, the regions with some degree of similarity to the TALEN target site were investigated. In detail, the genes including similar target regions were identified using BLAST in BdGDB (http://plantgdb.org/BdGDB/), isolated from the TALENed lines using the gene-specific primer pairs and sequenced to investigate off-target events.

Genomic DNA extraction, total RNA isolation and cDNA synthesis

Three independent plant samples were prepared for each tissue type. Prior to extraction of genomic DNA and total RNA, samples were ground in frozen mortars. DNA and RNA were extracted from *Brachypodium* seedlings using the standard CTAB method and an E.Z.N.A. Plant RNA Kit (Omega Biotek, Cat#R6827), respectively. Quality and quantity of extracted DNA and RNA from all samples were confirmed by both agarose gel visualization and spectrophotometry (Thermo Scientific, NanoDrop™ 1000). Total RNA samples were pretreated with recombinant DNase I to eliminate any contaminating genomic DNA and then were synthesized into primary cDNA using a PrimeScript™ RT reagent Kit with gDNA Eraser following the manufacturer's instructions (TaKaRa, Cat#RR047A).

Identification of mRNA alternative splicing events with reverse transcription PCR

To identify mRNA alternative splicing in *BdFTL1* and *BdFTL2* loci, reverse transcription PCR (RT-PCR) was used to amplify their full-length coding DNA sequence (CDS) using the primer

pairs, BdFTL1-CDS-F1/R1 and BdFTL2-CDS-F1/R1 (**Table S4**). RT-PCR was also used to isolate the complete CDS of *BdES43*. RT-PCR was performed in 25 μl reaction volumes comprising 2 μl of each primer (5 μM), 12.5 μl 2× PCR Mix (Xinhuitian Biotechnology, Cat#HT201), and 2.5 μl cDNA. PCR conditions were: 1 min at 94 °C, followed by 30 cycles of 10 sec at 94 °C, 20 sec at 65 °C, and 0.5 or 1 min at 72 °C, with a final extension of 5 min at 72 °C. PCR products were resolved by electrophoresis in 1 or 2% agarose gels, visualized using ethidium bromide (EB) staining, and photographed with the BioRad imaging system.

Quantitative real-time RT-PCR

The relative standard curve method was used when performing quantitative real-time RT-PCR (qPCR) experiments to obtain transcription patterns for genes of interest (Cao *et al*. 2011a). An ubiquitin-conjugating enzyme (*BdUBC18*, accession number: Bradi4g00660) in *Brachypodium* was a uniformly expressed control gene to calibrate the expression level of the genes of interest. A series of diluted genomic DNA were used to construct standard curve and calibrate PCR efficiencies. *BdFTL1*, *BdFTL2* and *BdES43* expression analyses were performed on cDNA samples collected from three biological replicates using the CFX Connect™ Real-Time System (Bio-Rad, http://www.bio-rad.com). Each primer pair spanned at least one intron to eliminate interference from genomic DNA. Each 25 μl qPCR mix included 12.5 μl SYBR Master Mix (Fermentas, Cat#K0223), 2.5 μl primer pair mix (2 μM for each primer) and 5 μl gDNA (gradient from 100 ng/μl to 0.032 ng/μl with a dilution factor of 5 for the standard curve) or cDNA as templates. Transcriptional patterns of *BdFTL1* and *BdFTL2* in the tissues of 4-week-old seedlings including roots, shoots and leaves, a time-course (0h, 4h, 8h, 12h, 16h, 20h, and 24h) of one day for the 3rd and 4th leaves of 4-week-old seedlings, and leaves of 1 to 6-week-old seedlings were investigated.

Y2H screen, BiFC and Pull-down assays

The full-length coding region of *BdFTL2* (Bradi1G48830) was directionally cloned into the Gateway™ entry vector pENTR™/D-TOPO® as described by the manufacturer and then shuttled into the destination vector pDEST32 using LR reaction (Invitrogen, Cat#K2400-20). The Y2H

screen was performed using the Gateway cDNA libraries constructed previously (Cao *et al*. 2011b). The partners (named "prey") of the protein of interest (named "bait") identified from Y2H library screening usually are retested to confirm their interaction. The "prey" vector of the partners were isolated and then re-transformed with the "bait" vector into yeast. BiFC experiments were carried out using the toolkit reported previously (Waadt *et al*. 2008). Full-length *BdFTL2* and *BdES43* were fused into pUC-SPYNE(R)173 and pUC-SPYCE(M), respectively. The resulting plasmids were co-transformed into *Brachypodium* protoplasts following the previously described procedure (Rincon-Arano *et al*. 2012). A confocal microscope was used to capture interaction signals following the procedure and parameter setting for YFP provided in the manufacturer's tutorial manual (Zeiss LSM700). The fluorescence can be emitted from exited chlorophyll just like YFP. Although the chlorophyll and YFP have different optimal excitation spectrums, 543 and 477 nm, respectively, the spectrum of 477 nm still can excite chlorophyll to emit, albeit weak, fluorescence. To exclude the interruption of chlorophyll, excitation spectrum of 543 nm was used to show the subcellular location of chloroplasts in wheat cells.

LUC assays also were used to validate the interaction between BdFTL2 and BdES43 as described previously (Chen *et al*. 2008; Song *et al*. 2011; Sun *et al*. 2013). Full-length coding regions of *BdFTL2* and *BdES43* were fused into pCAMBIA1300nLUC and pCAMBIA1300cLUC vectors, respectively. An *Agrobacterium tumefaciens* strain (GV3101) containing the resultant constructs was used to infiltrate *N. benthamiana* leaves. Luciferase activities in the leaves were determined 50 hours after infiltration. Fluorescence was monitored and imaged by LB985 NightSHADE (Berthhold Technologies) shortly after 100 µl of Luciferase assay substrate (Promega, Cat#E1500) were sprayed onto the infiltrated leaves.

For pull-down assays, BdFTL2 and BdES43 were fused with His and MBP tags, respectively, and expressed in *E. coli*. MBP is a natural affinity tag of amylose resin. As the H3K4me3 and H3K27me3 inputs, nuclear proteins were extracted from 3-week-old seedlings. Two grams of each tissue sample were ground into fine powder and then suspended in 10 ml of cold protein extraction buffer A [10 mM Hepes (Ph 7.9), 10 mM KCl, 0.2 mM EDTA, 1.5 mM $MgCl_2$, 1% N-40, 1 mM of DTT and 5% glycerol freshly mixed with 1 mM phenylmethylsulfonyl fluoride (PMSF), 3

mg/L Aprotinin, 3 mg/L Leupeptin and 2 mg/L Pepstain A]. The mixture including the fine powder of tissue samples and the above buffer A was incubated on ice for 15 min and then centrifuged at 2,800 × g for 10 min. The supernatant was discarded and the precipitant was re-suspended in 500 µl protein extraction buffer B [20 mM Hepes (pH 7.9), 420 mM KCl, 0.5 mM EDTA, 5 mM $MgCl_2$, 1% N-40, 1 mM DTT, and 10% glycerol freshly mixed with 1 mM PMSF, 3 mg/L Aprotinin, 3 mg/L Leupeptin and 2 mg/L Pepstain A]. The mixture including the above precipitant and protein extraction buffer B was incubated in ice for 30 min and then centrifuged at 20,000 × g for 5 min. The supernatant was harvested and incubated on ice. The purified BdES43-MBP was incubated with amylose resin (NEB, Cat#E8021S) at 4 °C for 1 hour and then mixed with the cold supernatant above or purified BdFTL2-His. The resulting mixtures were shaken gently for 4 hours and passed through a column to retain the resulting resin. Finally, the proteins were eluted from the resin. Protein blots were visualized using Immobilon Western Chemiluminescent HRP Substrate (Merck Millipore, Cat#WBKLS0100) with His antibody (Abbkine, Cat#A02050), H3K4me3 antibody (ABCAM, Cat#AB8580) or H3K27me3 antibody (ABCAM, Cat#AB6147).

ChIP-qPCR

For ChIP assays, overexpression lines of *BdES43* and *BdFTL2* were used to investigate the distribution of the target proteins at the target loci. *BdES43* and *BdFTL2* were fused with an YFP tag in the vector pEarleyGate 101. GFP antibody (ABCAM, Cat#AB6556), H3K4me3 antibody (ABCAM, Cat#AB8580) and H3K27me3 antibody (ABCAM, Cat#AB6147) are reactive against YFP, H3K4me3 and H3K27me3, respectively. H3K4me3 and H3K27me3 antibodies were also used to detect H3K4me3 and H3K27me3 distributions at the *BdFTL1* locus of WT lines during plant development. Protein A+G Agarose beads without antibody were used as non-immune controls (NIC). Sample preparation and experimental procedures for ChIP-qPCR assays were as described previously (Cao *et al*. 2014). In detail, 1 g leaf tissue was ground in liquid nitrogen and resuspended by 30 ml nuclear isolation buffer [10 mM HEPES (pH=7.6), 400 mM sucrose, 5 mM KCl, 5 mM $MgCl_2$, 5 mM EDTA, 1% formaldehyde, 14 mM 2-mercaptoethanol, 0.6% Triton

X-100, and 0.4 mM PMSF]. The lysate was crosslinked at room temperature for 10 min and was stopped by adding 2 ml Glycine (2 M). The lysate was filtered with the filter into a fresh tube. The nuclei was pelleted by centrifuging the filtrate at 2800 *g* for 10 min and dissolved in 200 µl nuclear lysis buffer [50 mM Tris–HCl pH 7.5, 1 % SDS, 10 mM EDTA (pH 8.0)]. The nuclei extract was loaded into sonicator (Bioruptor UCD200) and sonicated at the program of 30 s on/60 s off for 5 times. The sheared chromatin was centrifuged at 16,000 *g* for 5 min and the supernatant was transferred to a fresh tube. Subsequently, 30 µl protein A+G magnetic beads (Merck, Cat#16-663) together with 2 µg target antibody or IgG antibody (Non-immune control) as the negative control were added to the tube, and the mixture was rocked at 4°C overnight. After incubation, the beads was successively washed by 1 ml low salt immune complex wash buffer [0.1% SDS, 1.0% Triton X-100, 2 mM EDTA, 20 mM Tris-HCl (pH=8.0), 150 mM NaCl], 1 ml high salt immune complex buffer [0.1% SDS, 1.0% Triton X-100, 2 mM EDTA, 20 mM Tris-HCl (pH=8.0), 500 mM NaCl], 1 ml LiCl immune complex wash buffer [0.25 M LiCl, 1.0% NP-40, 1% sodium dexycholate, 1 mM EDTA, 10 mM Tris-HCl (pH=8.0)] and 1 ml TE, and eluted by 200 µl elution buffer (1% SDS, 100mM NaHCO3). The eluted immune complex was successively incubated at 65°C overnight together with 8 µl NaCl (5 M) and at 50°C for 2 h with 1 µl proteinase (Fermentas, Cat#EO049). The relative standard curve method was employed to test the enrichment of the target proteins at the target loci. Each 25 µl qPCR mix included 12.5 µl of SYBR Master Mix (Fermentas, Cat#K0223), 2.5 µl of primer pair mix (2 µM for each primer) and 5 µl gDNA (gradient from 100 ng/µl to 0.032 ng/µl with a dilution factor of 5 for the standard curve) or ChIPed DNA as templates. The qPCR profile was 2 min at 50 °C and 10 min at 95 °C, 45 cycles of 10 s at 95 °C, and 1 min at 60 °C followed by the default dissociation step for melt curves. All primers are listed in **Table S4**.

Statistical analyses

The mean values and error bars were calculated with the Excel functions “AVERAGE” and “STDEV”, respectively. Significant difference was determined by paired t-test using SigmaPlot 10. Multiple comparison analyses were conducted by Univariate Analysis of Variance

(UNIANOVA) in the general linear model using SPSS19. For multiple comparison of each gene, items for comparison were set as fixed factors and the underlying phenotypic data were used as independent variables. In the "Post Hoc" menu, the least significant difference (LSD) algorithm was selected to calculate statistical parameters for comparison.

Data availability statement

Sequence data from this article can be found in the GenBank/EMBL libraries under the following accession numbers: BdFTL1 (Bradi2g07070), BdFTL2 (Bradi1g48830), BdES43 (Bradi1g55090); BdmtN19 (Bradi3g41600), Bd2OG (Bradi1g51390), BdSTN7 (Bradi2g17660), BdB2 (Bradi2g40870), BdUPF06870 (Bradi2g41340) and BdUBC18 (Bradi4g00660) in BdGDB (http://plantgdb.org/BdGDB/).

Acknowledgments

We are grateful to Prof. R. A.McIntosh, Plant Breeding Institute, University of Sydney, for critical review of this manuscript. This work was supported by the Natural Science Foundation of China (91935304 and 31571663), National Key R&D program of China (2016YFD0100502) and the Gene Transformation Project (2016ZX08009003-004).

Author contributions

S.C. conceived the project and supervised this study. S.C., L.X. and X.L performed most of the experiments; C.G. participated in the material preparation and generation the transgenic lines; S.C., D.W., B.H., H.L., C.C. and X.X. wrote the paper. All the authors discussed the results and commented on the manuscript.

Competing interests

The authors declare that they have no competing interests.

Supporting legends

Figure S1 Identification of TALENed *BdFTL1* and *BdFTL2* lines.

Figure S2 Phenotypes of wild type (WT), *BdFTL1*-knockout (KO) and *BdFTL2*-KO lines under

short day (8h light/ 16h dark) conditions.

Figure S3 Open reading frame and alternative splicing pattern of *BdFTL1*.

Figure S4 Transcriptional patterns of *BdFTL1* in 1- to 3-week-old leaves from WT and *BdFTL2*-OE lines.

Figure S5 Transcription patterns of *Brachypodium FD* and *14-3-3* members and Y2H identification for the interaction between their encoded proteins and BdFTL2.

Figure S6 Sequence analyses of BdES43 homologs and the comparison of transcriptional activities between *BdES43* and *BdFTL2*.

Figure S7 Pull-down assays to investigate the interaction between BdES43 and H3k27me3.

Figure S8 Distribution of H3K4me3, H3K27me3 and BdES43 within *BdFTL2* locus of *BdES43*-OE lines.

Figure S9 Comparison of flowering time for WT, *BdFTL2*-OE, *BdFTL1*-KO and *BdFTL2*-OE/*BdFTL1*-KO lines under inductive LD conditions.

Table S1 Multiple comparisons and paired t-test for the spatial-temporal transcriptional activities of *BdFTL1* and *BdFTL2* based on qPCR arrays

Table S2 Interactors of BdFTL2 identified from Y2H screening in this study

Table S3 Multiple comparisons for the enrichment of target proteins at the *BdFTL1* locus based on ChIP-qPCR arrays

Table S4 Primers used in this study

Dataset S1 Sequences of the aligned items for FT homologs

Dataset S2 Syntenic genes around florigenic loci between *Brachypodium* and rice

Dataset S3 Multiple comparisons for the flowering time of transgenic lines

Dataset S4 TALEN sites designed for *BdFTL1* and *BdFTL2*

References

Adrian J. (2009) Transcriptional control of *FLOWERING LOCUS T* in *Arabidopsis*. PhD thesis, Max Planck Institute, Köln, German.

Alves S.C., Worland B., Thole V., Snape J.W., Bevan M.W. and Vain P. (2009) A protocol for *Agrobacterium*-mediated transformation of *Brachypodium distachyon* community standard line Bd21. Nat Protocol **4**(5):638-649.

Andres F. and Coupland G. (2012) The genetic basis of flowering responses to seasonal cues. Nature Review Genetics **13**(9):627-639.

Becker P.B. (2006) Gene regulation: a finger on the mark. Nature 442(7098):31-32.

Bell M.V., Cowper A.E., Lefranc M.P., Bell J.I. and Screaton G.R. (1998) Influence of intron length on alternative splicing of CD44. Molecular Cell Biology **18**(10):5930-5941.

Bentley D.L. (2014) Coupling mRNA processing with transcription in time and space. Nature Review Genetics **15**(3):163-175.

Bettgenhaeuser J., Corke F.M., Opanowicz M., Green P., Hernandez-Pinzon I. and Doonan J.H., and Moscou M.J. (2017) Natural variation in *Brachypodium* links vernalization and flowering time loci as major flowering determinants. Plant Physiology **173**: 256-268.

Braunschweig U., Gueroussov S., Plocik A.M., Graveley B.R. and Blencowe B.J. (2013) Dynamic integration of splicing within gene regulatory pathways. Cell **152**(6):1252-1269.

Brkljacic J., Grotewold E., Scholl R., Mockler T., Garvin D.F., Vain P., … and Vogel J.P. (2011) *Brachypodium* as a model for the grasses: Today and the future. Plant Physilogy **157**: 3-13.

Burnette J.M., Miyamoto-Sato E., Schaub M.A., Conklin J. and Lopez A.J. (2005) Subdivision of large introns in Drosophila by recursive splicing at nonexonic elements. Genetics **170**(2):661-674.

Cao S.H., Kumimoto R.W., Gnesutta N., Calogero A.M., Mantovani R. and Holt III B.F. (2014) A distal CCAAT/NUCLEAR FACTOR Y complex promotes chromatin looping at the FLOWERING LOCUS T promoter and regulates the timing of flowering in *Arabidopsis*.

Plant Cell **26**(3):1009-1017.

Cao S.H., Kumimoto R.W., Siriwardana C.L., Risinger J.R. and Holt III B.F. (2011a) Identification and characterization of NF-Y transcription factor families in the monocot model plant *Brachypodium distachyon*. PLoS One **6**(6):e21805.

Cao S.H., Siriwardana C.L., Kumimoto R.W. and Holt III B.F. (2011b) Construction of high quality Gateway entry libraries and their application to yeast two-hybrid for the monocot model plant *Brachypodium distachyon*. BMC Biotechnology **11**:53.

Chen H.M., Zou Y., Shang Y.L., Lin H.Q., Wang Y.J., Cai R., ... and Zhou J.M. (2008) Firefly luciferase complementation imaging assay for protein-protein interactions in plants. Plant Physiology **146**(2):368-376.

Christensen A.H., Sharrock .RA. and Quail P.H. (1992) Maize polyubiquitin genes: structure, thermal perturbation of expression and transcript splicing, and promoter activity following transfer to protoplasts by electroporation. Plant Molecular Biology **18**(4):675-689.

Corbesier L., Vincent C., Jang S., Fornara F., Fan Q.Z., Searle I., … and Coupland G. (2007) FT protein movement contributes to long-distance signaling in floral induction of *Arabidopsis*. Science **316**(5827):1030-1033.

Davie J.R., Xu W. and Delcuve G.P. (2016) Histone H3K4 trimethylation: dynamic interplay with pre-mRNA splicing. Biochemistry Cell Biology **94**(1):1-11.

de la Paz Sanchez M. and Gutierrez C. (2009) *Arabidopsis* ORC1 is a PHD-containing H3K4me3 effector that regulates transcription. National Academy of Sciences of USA **106**(6):2065-2070.

Ding Y., Ndamukong I., Xu Z.S., Lapko H., Fromm M. and Avramova Z. (2012) ATX1-generated H3K4me3 is required for efficient elongation of transcription, not initiation, at ATX1-regulated genes. PLoS Genetics **8**(12):e1003111.

Doyle E.L., Booher N.J., Standage D.S., Voytas D.F., Brendel V.P., Vandyk J.K. and Bogdanove A.J. (2012) TAL Effector-Nucleotide Targeter (TALE-NT) 2.0: tools for TAL effector design and target prediction. Nucleic Acids Researh **40**:W117-122.

Filichkin S.A., Priest H.D., Givan S.A., Shen R., Bryant D.W., Fox S.E., … and Mockler T.C. (2010) Genome-wide mapping of alternative splicing in *Arabidopsis thaliana*. Genome Research **20**(1):45-58.

Fornara F., de Montaigu A. and Coupland G. (2010) SnapShot: Control of flowering in Arabidopsis. Cell **141**(3):550-550.e552.

Fox-Walsh K.L., Dou Y, Lam B.J., Hung S.P., Baldi P.F. and Hertel K.J. (2005) The architecture of pre-mRNAs affects mechanisms of splice-site pairing. National Academy of Sciences of USA **102**(45):16176-16181.

Graveley B.R. (2005) Mutually exclusive splicing of the insect Dscam pre-mRNA directed by competing intronic RNA secondary structures. Cell **123**(1):65-73.

International Brachypodium Initiative (IBI) (2010) Genome sequencing and analysis of the model grass *Brachypodium distachyon*. Nature **463**(7282):763-768.

International Wheat Genome Sequencing Consortium (IWGSC) (2014) A chromosome-based draft sequence of the hexaploid bread wheat (*Triticum aestivum*) genome. Science **345**(6194):125178

Hatton A.R., Subramaniam V. and Lopez A.J. (1998) Generation of alternative Ultrabithorax isoforms and stepwise removal of a large intron by resplicing at exon-exon junctions. Molecular Cell **2**(6):787-796.

He Y. (2012) Chromatin regulation of flowering. Trends in Plant Science **17**(9):556-562.

Higgins J.A., Bailey P.C. and Laurie D.A. (2010) Comparative genomics of flowering time pathways using *Brachypodium distachyon* as a model for the temperate grasses. PLoS One **5**(4):e10065.

Huang Y., Min S., Lui Y., Sun J., Su X., Liu Y., … and Yang R. (2012) Global mapping of H3K4me3 and H3K27me3 reveals chromatin state-based regulation of human monocyte-derived dendritic cells in different environments. Genes and Immunity **13**(4):311-320.

Kandul N.P. and Noor M.A. (2009) Large introns in relation to alternative splicing and gene

evolution: a case study of *Drosophila* bruno-3. BMC Genetics **10**:67.

Kim E., Magen A. and Ast G. (2006) Different levels of alternative splicing among eukaryotes. Nucleic Acids Research **35**(1):125-131.

Kornblihtt A.R., Schor I.E., Alló M., Dujardin G., Petrillo E. and Muñoz M.J. (2013) Alternative splicing: a pivotal step between eukaryotic transcription and translation. Nature Review Molecular Cell Biology **14**(3):153-165.

Li C. and Dubcovsky J. (2008) Wheat FT protein regulates VRN1 transcription through interactions with FDL2. Plant Journal **55**(4):543-54.

Li C., Lin H. and Dubcovsky J. (2015) Factorial combinations of protein interactions generate a multiplicity of florigen activation complexes in wheat and barley. Plant Journal **84**(1):70-82.

López-González L., Mouriz A., Narro-Diego L., Bustos R., Martínez-Zapater J.M., Jarillo J.A. and Piñeiro M. (2014) Chromatin-dependent repression of the Arabidopsis floral integrator genes involves plant specific PHD-containing proteins. Plant Cell **26**(10):3922-3938.

Lu F.L., Cui X., Zhang S.B., Liu C.Y. and Cao X.F. (2010a) JMJ14 is an H3K4 demethylase regulating flowering time in Arabidopsis. Cell Research **20**(3):387-390.

Lu T., Lu G., Fan D., Zhu C., Li W., Zhao Q., … and Han B. (2010b) Function annotation of the rice transcriptome at single-nucleotide resolution by RNA-seq. Genome Research **20**(9):1238-1249.

Luco R. F., Pan Q., Tominaga K., Blencowe B. J., Pereira-Smith O. M., and Misteli T. (2010). Regulation of alternative splicing by histone modifications. Science (New York, N.Y.), **327**(5968), 996–1000.

Lv B., Nitcher R., Han X., Wang S., Ni F., Li K., … and Fu D. (2014) Characterization of *FLOWERING LOCUS T1* (*FT1*) gene in *Brachypodium* and wheat. PLoS One **9**(4):e94171.

Mcguire A.M. (2008) Cross-kingdom patterns of alternative splicing and splice recognition. Genome Biology **9**(3):R50.

Mercer T.R., Edwards S.L., Clark M.B., Neph S.J., Wang H., Stergachis A.B., … and

Stamatoyannopoulos J.A. (2013) DNase I-hypersensitive exons colocalize with promoters and distal regulatory elements. Nature Genetics, **45**(8), 852–859.

Molitor A.M., Bu Z., Yu Y. and Shen W.H. (2014) *Arabidopsis* AL PHD-PRC1 Complexes promote seed germination through H3K4me3-to-H3K27me3 chromatin state switch in repression of seed developmental genes. PLoS Genetics **10**(1):229-231.

Navarro C., Cruz-Oro E. and Prat S. (2015) Conserved function of FLOWERING LOCUS T (FT) homologues as signals for storage organ differentiation. Current Opinion Plant Biology **23**:45-53.

Ong-Abdullah M., Ordway J.M., Jiang N., Ooi S.E., Kok S.Y., Sarpan N., … and Martienssen R.A. (2015) Loss of Karma transposon methylation underlies the mantled somaclonal variant of oil palm. Nature **525**(7570):533-537

Pandya-Jones A. and Black D.L. (2009) Co-transcriptional splicing of constitutive and alternative exons. RNA **15**(10):1896-1908.

Pin P.A. and Nilsson O. (2012) The multifaceted roles of *FLOWERING LOCUS T* in plant development. Plant Cell Environment **35**(10):1742-1755.

Qian S., Lv X., Scheid R.N., Lu L., Yang Z., Chen W., … and Du J. (2018) Dual recognition of H3K4me3 and H3K27me3 by a plant histone reader SHL. Nature Communications **9**(1): 2425.

Qin Z., Wu J., Geng S., Feng N., Chen F., Kong X., … and Wu L. (2017) Regulation of *FT* splicing by an endogenous cue in temperate grasses. Nature Communications **8**:14320.

Ream T.S., Woods D.P., Schwartz C.J., Sanabria C.P., Mahoy J.A., Walters E.M., ,… and Amasino R.M. (2014) Interaction of photoperiod and vernalization determines flowering time of *Brachypodium distachyon*. Plant Physiology **164**(2):694-709.

Rincon-Arano H., Halow J., Delrow J.J., Parkhurst S.M. and Groudine M. (2012) UpSET recruits HDAC complexes and restricts chromatin accessibility and acetylation at promoter regions. Cell **151**(6):1214-1228.

Roy M., Kim N., Xing Y. and Lee C. (2008) The effect of intron length on exon creation ratios

during the evolution of mammalian genomes. RNA (New York, N.Y.) **14**(11):2261-2273.

Schwartz C.J., Doyle M., Manzaneda A.J., Rey P.J., Mitchell-Olds T. and Amasino R.M. (2010) Natural variation of flowering time and vernalization responsiveness in *Brachypodium distachyon*. Bioenergy Research **3**(1):38-46.

Shan Q., Wang Y., Chen K., Liang Z., Li J., Zhang Y., … and Gao C. (2013) Rapid and efficient gene modification in rice and *Brachypodium* using TALENs. Molecular Plant **6**(4):1365-1368.

Shi X., Hong T., Walter K.L., Ewalt M., Michishita E., Hung T., … and Gozani O. (2006) ING2 PHD domain links histone H3 lysine 4 methylation to active gene repression. Nature **442**(7098):96-99.

Shukla S. and Oberdoerffer S. (2012) Co-transcriptional regulation of alternative pre-mRNA splicing. Biochimica et Biophysica Acta **1819**(7):673-683.

Song S., Qi T., Huang H., Ren Q., Wu D., Chang C., … and Xie D. (2011) The Jasmonate-ZIM domain proteins interact with the R2R3-MYB transcription factors MYB21 and MYB24 to affect Jasmonate-regulated stamen development in *Arabidopsis*. Plant Cell **23**(3):1000-1013.

Song Y.H., Shim J.S., Kinmonth-Schultz H.A. and Imaizumi T. (2015) Photoperiodic flowering: time measurement mechanisms in leaves. Annual Review Plant Biology **66**:441-464.

Spies N., Nielsen C.B., Padgett R.A. and Burge C.B. (2009) Biased chromatin signatures around polyadenylation sites and exons. Molecular Cell **36**(2):245-254.

Srikanth A. and Schmid M. (2011) Regulation of flowering time: all roads lead to Rome. Cell Molecular Life Sciences **68**(12):2013-2037.

Sun J., Qi L., Li Y., Zhai Q. and Li C. (2013) PIF4 and PIF5 transcription factors link blue light and auxin to regulate the phototropic response in *Arabidopsis*. Plant Cell **25**(6):2102-2114.

Tamada Y., Yun J.Y., Woo S.C. and Amasino R.M. (2009) ARABIDOPSIS TRITHORAX-RELATED7 is required for methylation of lysine 4 of histone H3 and for transcriptional activation of *FLOWERING LOCUS C*. Plant Cell **21**(10):3257-3269.

Tamaki S., Matsuo S., Wong H.L., Yokoi S. and Shimamoto K. (2007) Hd3a protein is a mobile flowering signal in rice. Science **316**(5827):1033-1036.

Taoka K., Ohki I., Tsuji H., Kojima C. and Shimamoto K. (2013) Structure and function of florigen and the receptor complex. Trends in Plant Sciences **18**(5):287-294.

Tian Y., Jia Z., Wang J., Huang Z., Tang J., Zheng Y., … and Ni B. (2011) Global mapping of H3K4me1 and H3K4me3 reveals the chromatin state-based cell type-specific gene regulation in human Treg cells. PLoS One **6**(11):e27770.

Waadt R., Schmidt L.K., Lohse M., Hashimoto K., Bock R. and Kudla J. (2008) Multicolor bimolecular fluorescence complementation reveals simultaneous formation of alternative CBL/CIPK complexes in planta. Plant J **56**(3):505-516.

Wigge P.A. (2011) FT, a mobile developmental signal in plants. Current Biology **21**(9):R374-378.

Woods D.P., Ream T.S., Minevich G., Hobert O. and Amasino R.M. (2014) PHYTOCHROME C is an essential light receptor for photoperiodic flowering in the temperate grass, *Brachypodium distachyon*. Genetics **198**, 397-408.

Wu L., Liu D., Wu J., Zhang R., Qin Z., Liu D., … and Mao L. (2013) Regulation of *FLOWERING LOCUS T* by a microRNA in *Brachypodium distachyon*. Plant Cell **25**(11):4363-4377.

Wysocka J., Swigut T., Xiao H., Milne T.A., Kwon S.Y., Landry J., … and Allis C.D. (2006) A PHD figner of NURF couples histone H3 lysine 4 trimethylation with chromatin remodelling. Nature **442**(7098):86-90.

Yang H., Mo H., Fan D., Cao Y., Cui S. and Ma L. (2012) Overexpression of a histone H3K4 demethylase, JMJ15, accelerates flowering time in *Arabidopsis*. Plant Cell Report **31**(7):1297-1308.

Yu C.W., Liu X., Luo M., Chen C., Lin X., Tian G., … and Wu K. (2011) HISTONE DEACETYLASE6 interacts with FLOWERING LOCUS D and regulates flowering in *Arabidopsis*. Plant Physiology **156**(1):173-184.

Zhang, Y., Zhang, F., Li, X., Baller, J.A., Qi, Y., … and Voytas, D.F. (2013). TALENs enable

efficient plant genome engineering. Plant Physiology, **161**(1):20-27

Figure legends

Figure 1 Phylogenetic and synteny analyses of FT homologs. (A) Neighbor-joining tree of FT and related proteins in *Brachypodium distachyon* (Bd), *Triticum aestivum* (Ta), *Hordeum vulgare* (Hv), *Oryza sativa* (Os), *Setaria italica* (Si), *Sorghum bicolor* (Sb), *Zea mays* (Zm) and *Arabidopsis thaliana* (At). The phylogenic tree was constructed based on the multiple alignments of protein conserved regions using the software Clusal W following Higgins *et al* (2010). The purple box shows the sub-branch including functionally validated FT proteins. All *Brachypodium* FT homologs are underlined. (B) Collinearity analysis of *FT* gene-containing region in rice chromosome 1 with the orthologous regions of *Brachpodium* chromosome 2. (C) Collinearity analysis of *FT* gene-containing region in rice chromosome 6 with the orthologous regions of *Brachypodium* chromosome 1. Note: here the names of *Brachypodium* FT homologs follow the rice nomenclature system.

Figure 2 Phenotypes of *BdFTL1* and *BdFTL2* overexpression and knockout lines.

(A) Phenotypes of transgenic lines of *BdFTL1* and *BdFTL2* driven by the ZmUbi promoter. pUb1-BdFTL1 and pUbi-BdFTL2 represent the constructs of ZmUbi promoter-driven *BdFTL1* and *BdFTL2*, respectively. (B) Representative plants from transgenic lines of *BdFTL1* and *BdFTL2* driven by the 35S promoter. The representative plants for wild type (WT), *BdFTL1* OE and *BdFTL2* OE lines are approximately 45, 25 and 25 days old, respectively, post seed germination. (C) Days to flowering of WT, *BdFTL1*-OE and *BdFTL2*-OE lines. (D) Representative plants for *BdFTL1* knockout (KO) and *BdFTL2*-KO lines. The two independent lines for each of *BdFTL1* KO and *BdFTL2* KO were used to display their phenotypes. The representative plants for WT, *BdFTL1* KO, *BdFTL2* KO and double KO are approximately 45, 45, 140 and 140 days old, respectively. (E) Days to flowering of WT, *BdFTL1*-KO and *BdFTL2*-KO lines. * labeled significant difference at $P = 0.05$. The double mutants of *BdFTL1* and *BdFTL2* were generated from the hybridization between their respective mutant lines. *BdFTL1* KO lines had comparable flowering times to WT lines **(*P* = 0.054 in Dataset S3)**. Flowering times of

BdFTL2 KO lines were not significantly different from those of the double mutants **(*P* = 0.054 in Dataset S3)**. The transcriptional level of *BdFTL1* showed the total of normal and AS transcripts using qPCR with a primer pair targeting the overlapping region of the two transcripts (**Figure S3; Table S4**).

Figure 3 Transcriptional patterns and AS events for *BdFTL1* and *BdFTL2* under inductive long day (LD) conditions.

Transcriptional patterns of *BdFTL1* and *BdFTL2* in (A) tissues of 4-week-old seedlings, (B) a time-course of one day for 3rd and 4th leaves of 4-week-old seedlings; Z0~24: Zeitgeber 0~24, (C) over six weeks; 1 to 6-week-old leaves were used. Paired t-tests show that *BdFTL1* and *BdFTL2* have similar tissue-specific expression profiles **(*P* = 0.0578 in Table S1)**, parallel transcriptional patterns during a time-course over a full day **(*P* = 0.1489 in Table S1)** and consistent transcriptional variation over different developmental phases **(*P* = 0.7186 in Table S1)**. (D) Detection of AS products from the *BdFTL1* locus under inductive LD conditions during developmental processes. Samples were the same as those used in (C). Red and blue arrows show the functional transcript with the complete coding DNA sequence (its function to promote flowering was identified by overexpression experiments in **Figure 2A**) and the AS-derived isoform with a premature stop codon, respectively. M: DL2000 DNA marker (Takara) including DNA fragments of 2000, 1000, 750, 500 and 250 bp (from top to bottom). The bands in the lower part of this panel is the target fragment amplified from *BdUBC18*, which acted as an internal reference to calibrate the expression level of *BdFTL1*. (E) No AS event was observed at the *BdFTL2* locus. Here the samples, marker and internal gene were the same as those in (D). (F) Transcriptional patterns of *BdFTL1* in 1- to 7-week-old leaves from WT and *BdFTL2*-KO lines, respectively. The qPCR curve showed the total transcription pattern of all splicing variants. (G) Transcriptional activities and AS events 1- to 14-week-old leaves of *BdFTL1* in *BdFTL2*-KO lines under inductive LD conditions during plant development. Red and blue arrows, the samples, marker and internal gene were the same as those in (D).

Figure 4 BdFTL2 interacts with BdES43 in targeting H3K4me3. (A) Interacting BdFTL2

partners identified by Y2H screens; 1: BdmtN19 (Bradi3g41600), 2: BdES43 (Bradi1g55090), 3: Bd2OG (Bradi1g51390), 4: BdSTN7 (Bradi2g17660), 5: BdB2 (Bradi2g40870), 6: BdUPF06870 (Bradi2g41340). CK(+) and CK(-) represent the manufacturer's (Invitrogen) positive and negative controls, respectively. These partners of BdFTL2 identified from Y2H screening are retested to confirm their interaction with BdFTL2 in yeast. (B) Bimolecular fluorescence complementation (BiFC) experiments to investigate interaction of BdFTL2 and BdES43 in *Brachypodium* protoplasts. YC + BdFTL2-YN and YN + BdES43-YC are negative controls (NC). Compared to NC, BdFTL2-YN + BdES43-YC can generate observable signals in the nuclei of the protoplasts, showing they can interact in *Brachypodium* protoplasts. Pink arrows show the location of nuclei in Bright fields. (C) Pull-down assays to validate physical interaction between BdFTL2 and BdES43. M: protein marker (GenStar, M221-05). BdFTL2 and BdES43 were fused with His and MBP tags, respectively, and expressed in *E. coli*. Amylose resin was used as an affinity matrix to isolate the proteins fused to maltose-binding protein (MBP). The interaction of BdFTL2 and BdES43 *in vitro* was detected by Western blot with His antibody. (D) Luciferase complementation (LUC) experiments in tobacco to confirm the interaction between BdFTL2 and BdES43. The regions infiltrated with BdFTL2-cLUC/nLUC, BdES43-nLUC/cLUC or nLUC/cLUC were negative controls (NC). No signal was detected in the NC regions, while signals could be observed in the region infiltrated with BdFTL2-cLUC/BdES43-cLUC, showing they can bind *in planta*. (E) Pull-down assays to validate interaction between BdES43 and H3K4me3. BdES43 were fused with MBP tag and expressed in *E. coli*. As the H3K4me3 input, nuclear proteins were extracted from 3-week-old seedlings. Western blot detected by H3K4me3 antibody showed that BdES43 could bind H3K4me3 *in vitro*. (F) Phenotypic traits of 35S-driven *BdES43*-OE lines. The representative plants for WT, *BdFTL2* OE and *BdES43* OE are 45, 25 and 45 days old, respectively, post seed germination. (G) Days to flowering of WT, *BdFTL2* OE and *BdES43* OE lines. (H) Comparison of *BdFTL1* and *BdFTL2* transcription patterns between wild-type and *BdES43*-OE lines under inductive LD conditions during developmental processes; 1~7 week-old leaves are used.

Figure 5 BdFTL2 regulates *BdFTL1* by binding with the BdES43-H3K4me3 complex. (A)

Schematic of the *BdFTL1* locus showing primer-targeted sites for ChIP-qPCR experiments. The downward arrows show the AS site and the red right arrow indicates the location of the transcriptional start site (TSS). The TSS is located at approximately 146 bp upstream to the start codon ATG and is predicted using TSSP (http://www.softberry.com/berry.phtml?topic=tsspandgroup=programsandsubgroup=promoter). The black rectangles and black lines show the exons and introns, respectively. The black lines with white dots indicate the promoter of *BdFTL1* and the distance between two adjacent dots is 100 bp. (B) H3K4me3 H3K27me3, and BdES43 distributions within the *BdFTL1* locus. The promoter plus AS region (represented by I, II, III, IV and V regions) and more distal locations (represented by VI, VII and VIII regions) of *BdFTL1* locus were highlighted in pink and blue, respectively. The two-week-old seedlings of *BdES43*-OE lines were used. (C) H3K4me3 H3K27me3, and BdFTL2 distribution within the *BdFTL1* locus of *BdFTL2*-OE lines. The promoter plus AS region (represented by I, II, III, IV and V regions) and more distal locations (represented by VI, VII and VIII regions) of *BdFTL1* locus were highlighted in pink and blue, respectively. The two-week-old seedlings of *BdFTL2*-OE lines were used. (D) H3K4me3 distribution within the *BdFTL1* locus of WT lines at different stages of development. (E) H3K27me3 distribution within *BdFTL1* locus of WT line at different stages of development.

Figure 6 Flowering regulatory models underlying BdES43 interaction with BdFTL2. (A) The working model of BdFTL2 regulating *BdFTL1* transcription and AS through interacting with BdES43. U1: mRNA splicing complex; pol II: RNA polymerase II transcription complex. *FTL1*: *BdFTL1* locus; FTL2: BdFTL2 protein; PHD: BdES43 protein. (B) The working model of BdES43 vying with BdFDL or/and Bd14-3-3 members for BdFTL2 to regulate flowering time. FDL: BdFDL protein; 14-3-3: Bd14-3-3 protein.

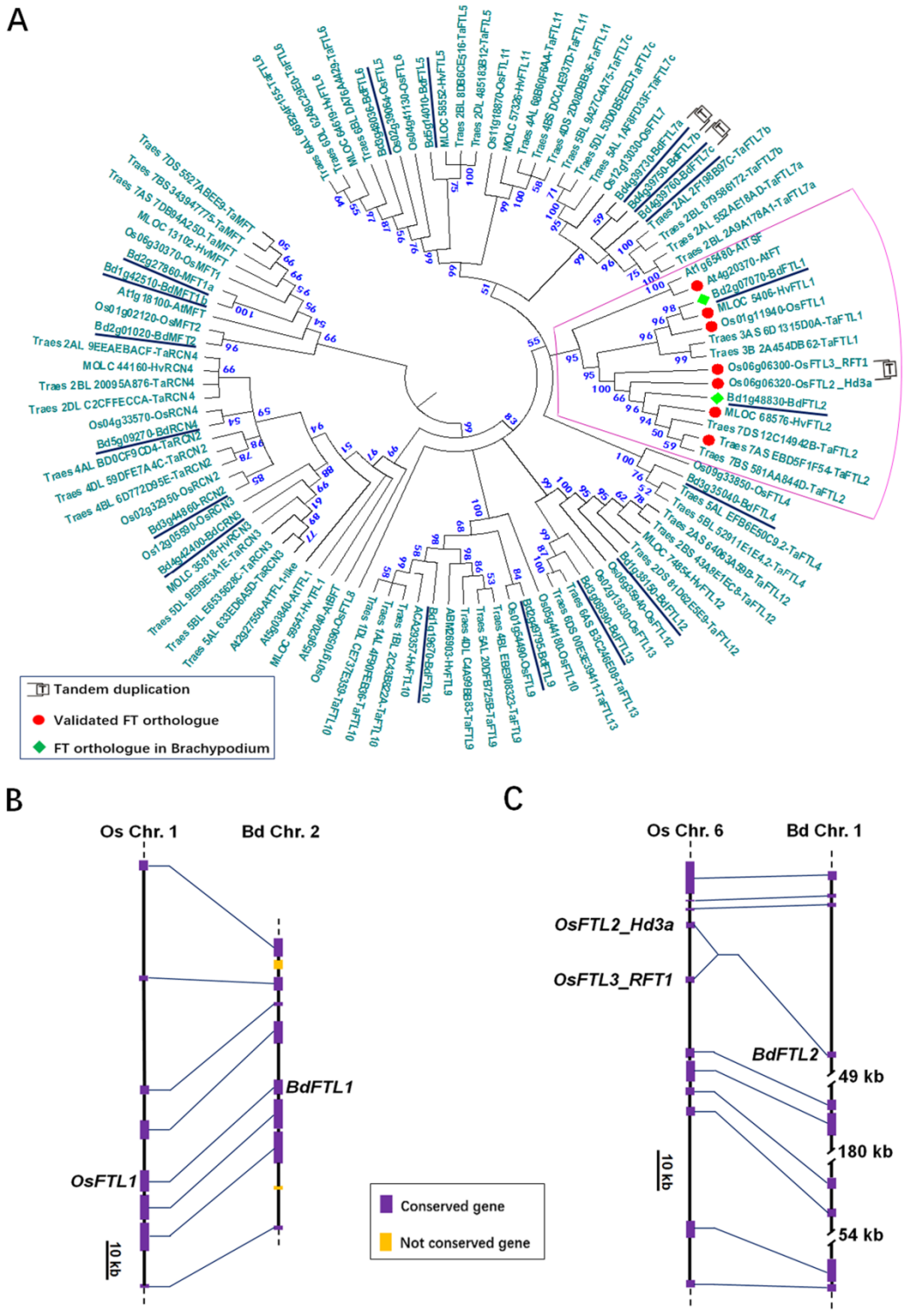

tpj_14622_f1.png

A

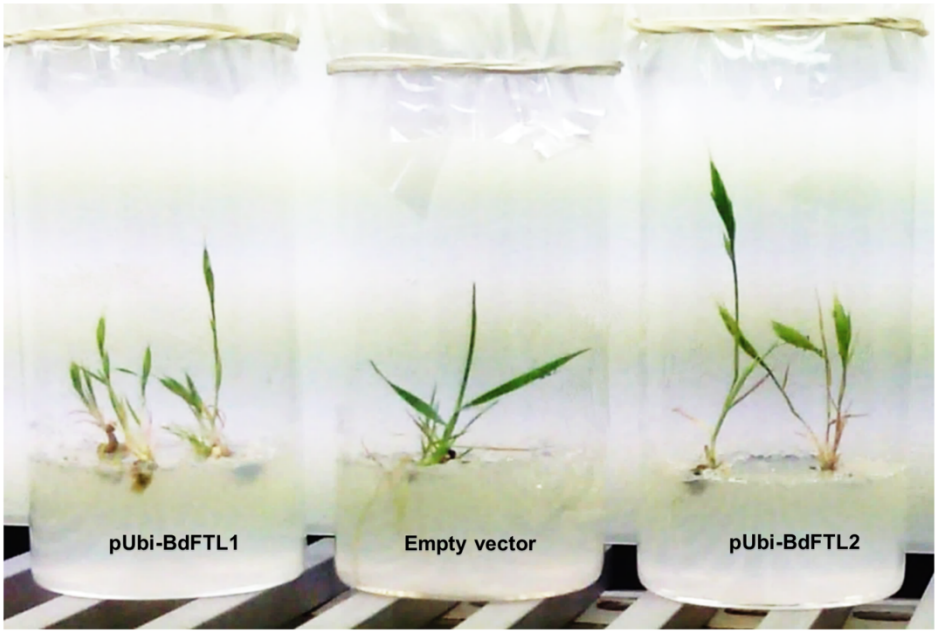

B

C

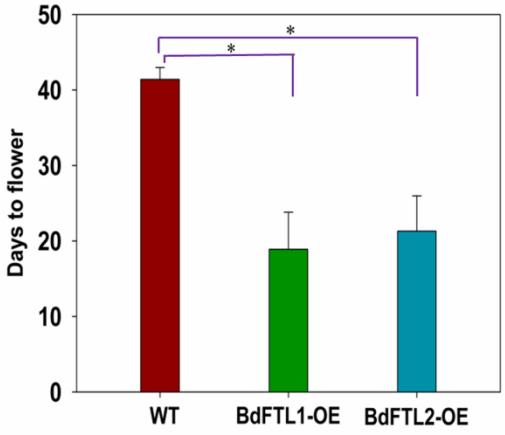

D

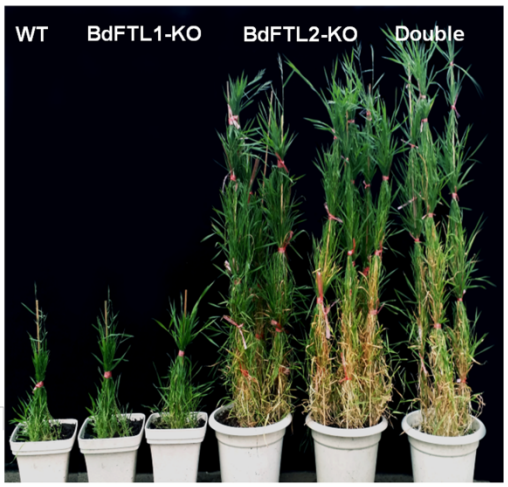

E

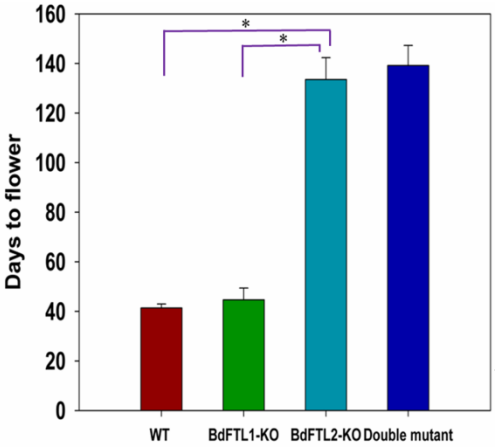

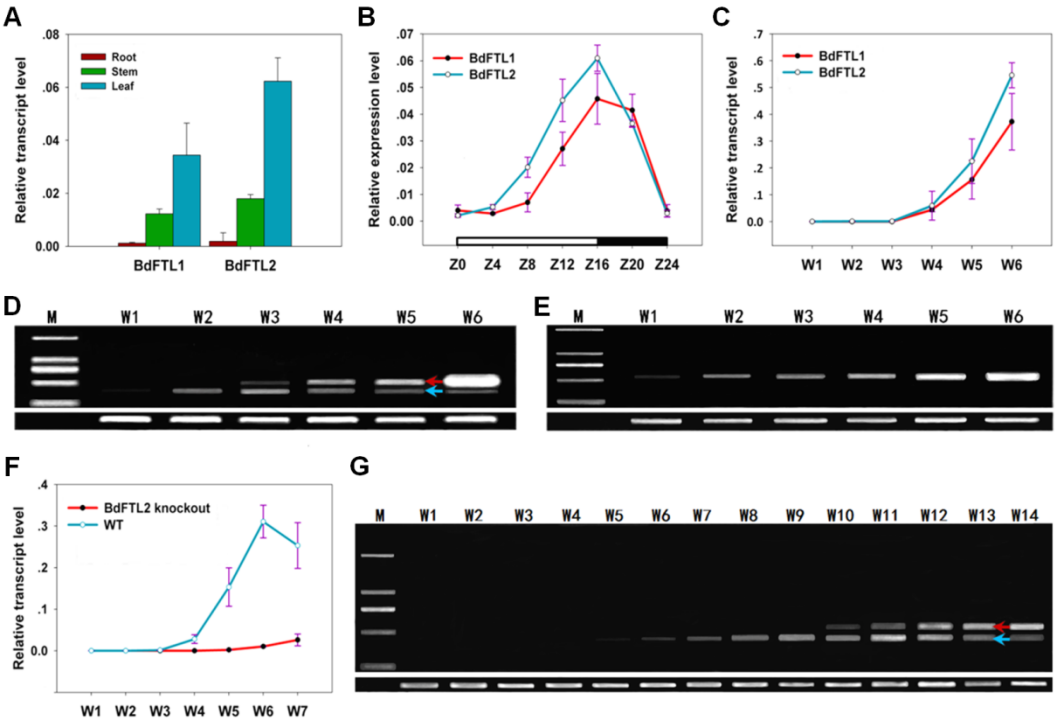

tpj_14622_f3.png

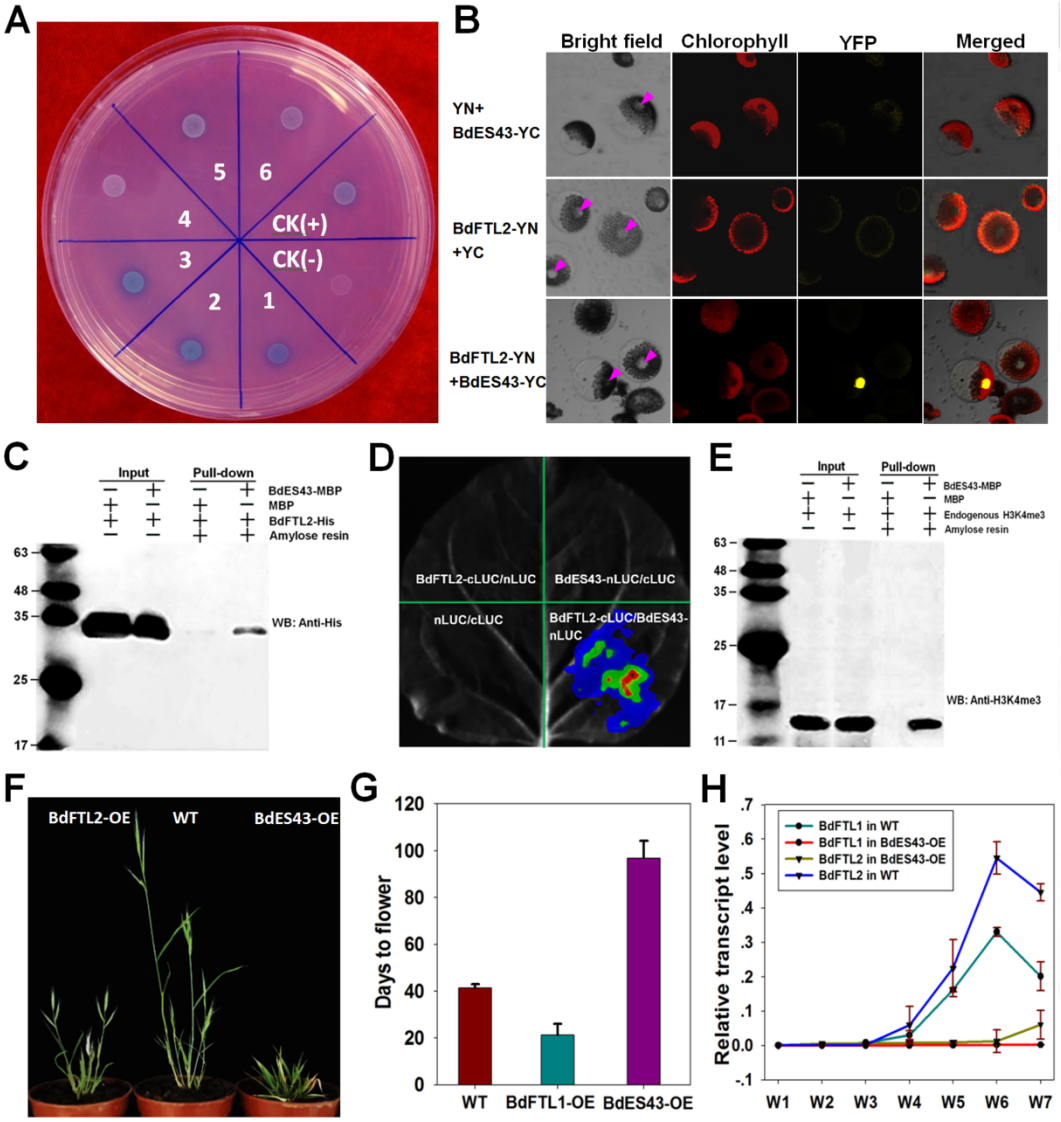

tpj_14622_f4.png

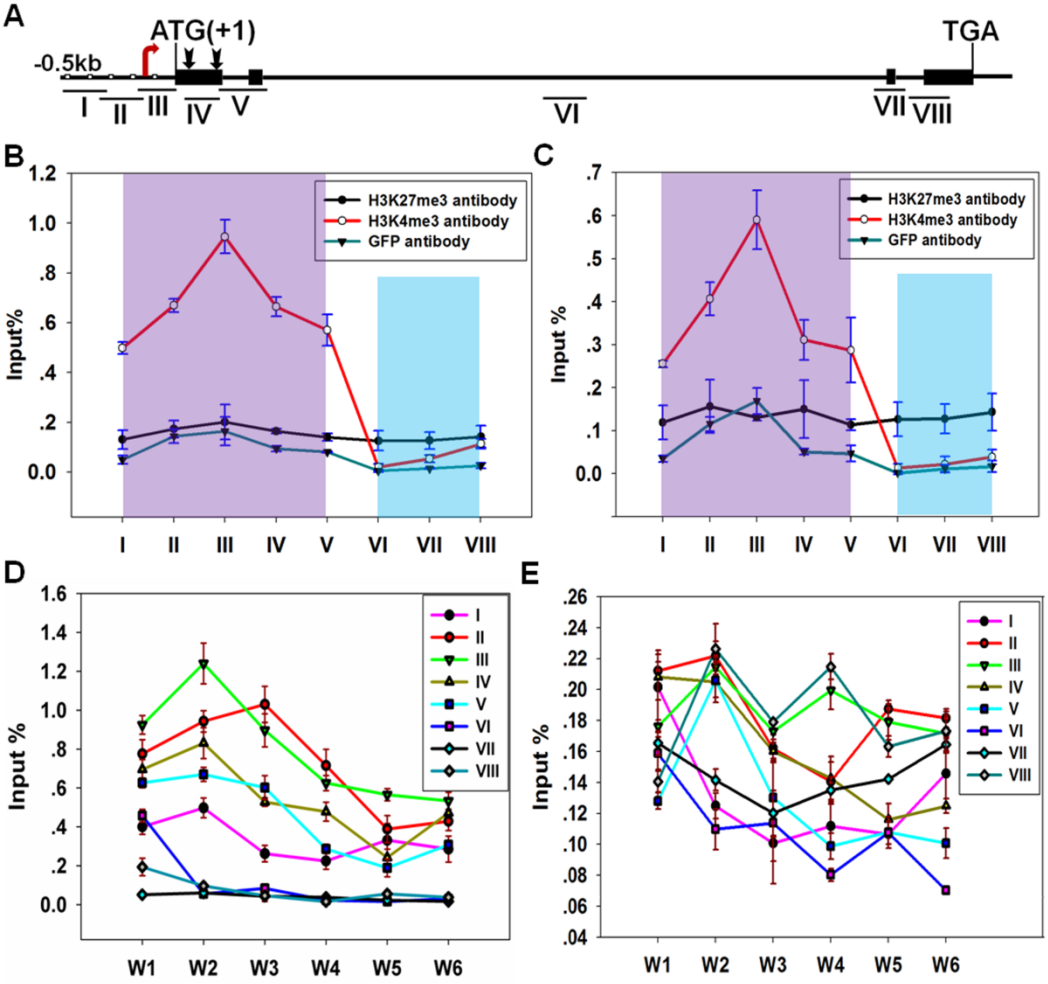

tpj_14622_f5.png

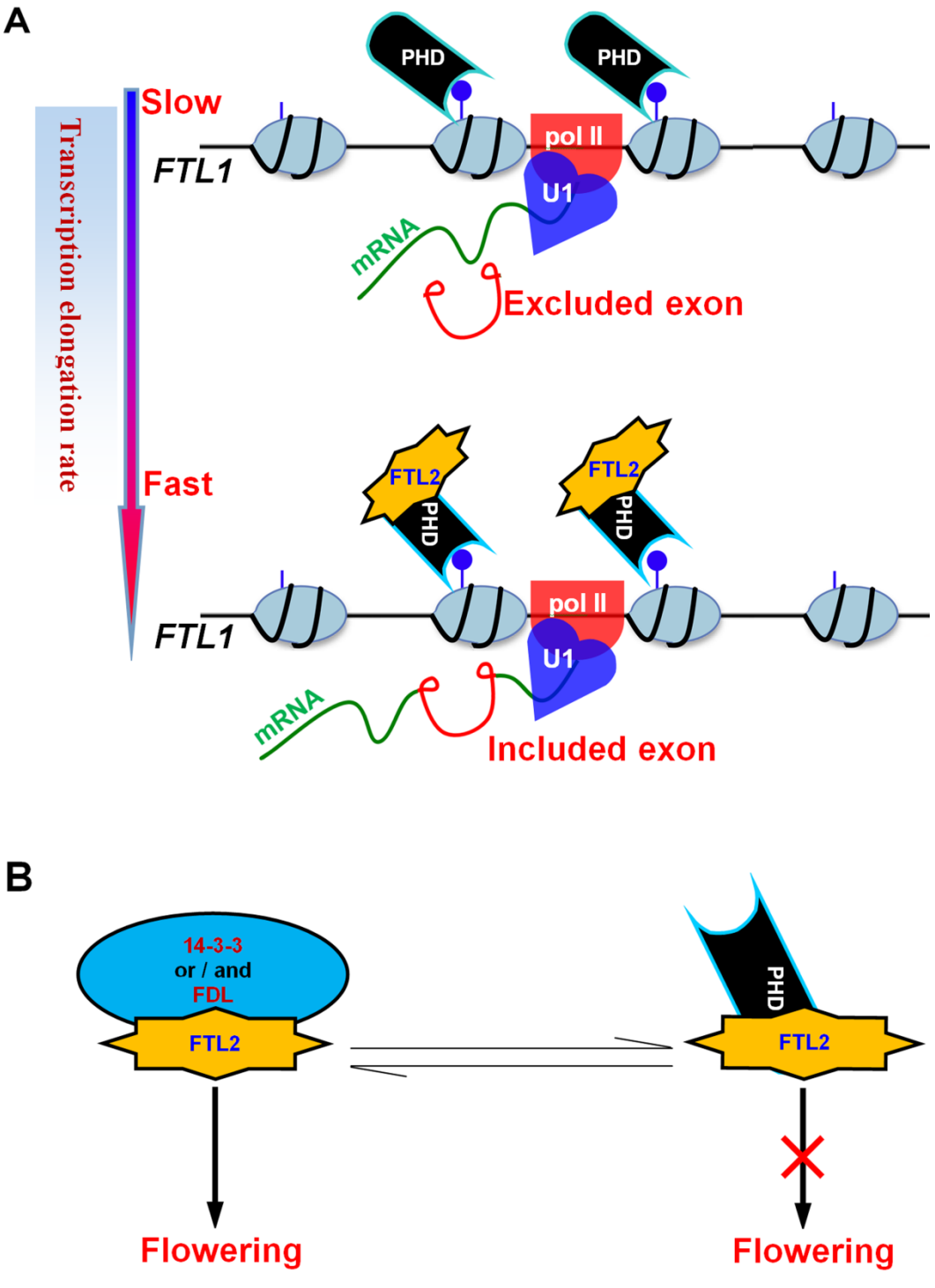

tpj_14622_f6.png